Industrial Crops and Products xxx (2014) xxx–xxx

Contents lists available at ScienceDirect

Industrial Crops and Products

journal homepage: www.elsevier.com/locate/indcrop

Investigation of microstructure and tensile properties of porous natural coir fibre for use in composite materials

L.Q.N. Tran [a,b,*], T. Nguyen Minh [c], C.A. Fuentes [b], T. Truong Chi [c], A.W. Van Vuure [b], I. Verpoest [b]

[a] Singapore Institute of Manufacturing Technology, Agency for Science, Technology and Research (A*STAR), Singapore
[b] Department of Materials Engineering (MTM), KU Leuven, Leuven, Belgium
[c] Department of Chemical Engineering, Can Tho University, Viet Nam

ARTICLE INFO

Article history:
Received 4 June 2014
Received in revised form 29 October 2014
Accepted 30 October 2014
Available online xxx

Keywords:
Natural fibres
Microstructure
Tensile properties
X-ray tomography

ABSTRACT

Natural coir fibres are studied for use as reinforcement in composite materials. In order to efficiently use the fibres and understand the composite properties, the microstructure and the mechanical properties of coir fibres are investigated in this study. X-ray microtomography in SEM (SEM-CT) and SEM image analysis are used to examine the fibre internal structure including the organisation of elementary fibres, microfibril angles and fibre porosity. Mechanical properties of coir fibres are determined by performing fibre tensile tests, in which an integrated optical strain mapping system is used to define fibre strain for producing more reliable values of *E*-modulus and strain at failure. The results show that technical coir fibres comprise plenty of elementary fibres and a lacuna at the centre. The elementary fibre is built up by two main cell walls which consist of bundles of microfibrils with a large misorientation with respect to the elementary fibre axis. Coir fibres appear to have a high porosity of 22 to 30%. The high microfibrillar angle in the coir fibres leads to the low stiffness in fibre direction and to high elongation to failure thanks to reorientation of the microfibrils under tensile loading.

1. Introduction

Natural fibres have recently attracted the interest as composite material reinforcement, thanks to their good mechanical properties in combination with lightweight. Additionally, they have environment-friendly characteristics such as low energy utilisation, renewability and biodegradability. As extracted from natural plants, natural fibres have a variation in mechanical properties which are mainly attributed to the microstructure and chemical composition of the fibres. To efficiently use natural fibres in composite materials, it is necessary to investigate the morphology, structure and mechanical properties of the fibres, which influence the properties of their composites.

The natural fibres used in composites are commonly defined as technical fibres. A technical natural fibre consists of several cells referred to as elementary fibres. The elementary fibre is mainly formed out of multiple cellulose–lignin/hemicellulose cell wall layers, in which crystalline microfibrils based on cellulose are connected into the cell wall layer by amorphous lignin and hemicelluloses (Bledzki and Gassan, 1999; Burgert, 2006; Fengel and Wegener, 1989; Lefeuvre et al., 2014). The cell wall layers can have different thickness, chemical organisation and orientation of the cellulose microfibrils (microfibrillar angle – MFA) (Burgert, 2006; Müssig and Stevens, 2010; Tomczak, 2007).

The mechanical properties of natural fibres depend on the organisation of the cell walls with regard to cell wall/lumen ratio and the cellulose MFA in the dominant cell wall layers. In relation with fibre cross-section, higher density fibres are stiffer and stronger than the lower density ones. The elastic modulus and strain at failure of fibres are also dependent on the MFA. A small MFA, in which cellulose microfibrils are oriented almost parallel to the axial direction, leads to a high modulus of elasticity, whereas the stiffness is substantially decreased for higher MFA's (Lefeuvre et al., 2014; Navi et al., 1995; Page et al., 1971).

The mechanical properties of fibres can be determined by tensile testing of either individual (single) fibres or fibre bundles. The single fibre tensile tests have been applied on a wide number of natural fibres including flax, hemp, jute, bamboo and coir (Baley, 2002; Martin et al., 2013; Osorio et al., 2011; Pickering et al., 2007; Silva et al., 2000), in which the fibre is usually glued onto a paper

* Corresponding author at: Singapore Institute of Manufacturing Technology; Agency for Science, Technology and Research (A*STAR), Singapore.
Tel.: +65 67938958; fax: +65 67925362.
E-mail address: tranlqn@simtech.a-star.edu.sg (L.Q.N. Tran).

http://dx.doi.org/10.1016/j.indcrop.2014.10.064
0926-6690/

frame with a fixed test length. The test length varies from 1 mm in the study of Snell et al. (1993) to 50 mm reported in Silva et al. (2000), depending on the fibre structure. The latter method is dry fibre bundle tensile test, which was initially developed for characterisation of synthetic fibres (Chi et al., 1984; Coleman, 1958), and later applied on natural fibres (Trujillo et al., 2014). In most cases, it is not possible to use an extensometer for measuring fibre strain due to the small dimensions involved. For single fibre testing, Defoirdt et al. (2010) have presented a correction method for single fibre tensile tests to determine the real elongation of the fibre when only the registered displacement of the clamps is available. The method is however time consuming because a high number of single fibre tensile tests has to be carried out at various test lengths.

The aim of this work is to study the microstructure and the tensile mechanical properties of technical coir fibres. SEM and X-ray microtomography in SEM (SEM-CT) are used to examine the fibre internal structure and fibre porosity. The mechanical properties of coir fibres are then determined in tensile tests integrated with optical strain mapping. The relation between fibre structure and fibre properties will be discussed based on the results of the above analysis.

2. Experimental

2.1. Coir fibres

Coir fibres used in this research are long coir fibres (fibre length in the range of 200–300 mm) which were provided by Can Tho University – Vietnam. The fibres were mechanically extracted from husk shells of premature and mature coconuts (10–12 months on the plant) with a purely mechanical extraction process, which can keep the fibre as long as possible. There was not any retting or chemical treatment applied before extracting the fibres. The fibres are then soaked in hot water at 70 °C for 2 h, washed with ethanol, rinsed with deionized water and dried in a vacuum oven at 90 °C. These fibres were preserved in a conditioned room at 25 °C and humidity of 50% for later studies.

2.2. Investigation of the fibre microstructure using SEM and SEM-CT

For the analysis of the internal fibre structure and the fibre porosity, both SEM and SEM-CT were used for characterisation on the same fibre samples, and the results from the two methods were compared.

In the first method, SEM images of three different cross-sections were taken for each fibre. With the help of the software Leica QWin, the area of the fibre cross-section and the lumens were determined. These data were also used for the calculation of the fibre porosity based on the ratio between the porous area and the area of the fibre section.

The second method was X-ray tomography scanning of the fibre segments by SEM-CT, with the SkyScan micro-CT attachment for the XL30 SEM. Titanium was used as a target in combination with 30 kV voltage on the electron beam to generate X-rays. The entire fibre segment was scanned, and then a full volumetric image was obtained after reconstructing the scanned images by using the SkyScan NRecon software. With these sets of data, morphological measurement of the fibre in 2D and 3D was carried out with the help of the SkyScan CTanalyser software. In the tomography scanning, in order to obtain high resolution images, the X-ray beam is generated with low power (30 kV) and high current of 120 μA, in combination with long exposure time of 4000 ms.

Regarding the number of test fibres, it should be noted that the extracted technical coir fibres naturally present as such as in the coconut husk. They are quite similar and less variation in terms of fibre structure and fibre properties, as compared to other natural fibres (e.g. flax, jute and bamboo). In this study, ten fibre samples were characterised using the two methods.

2.3. Measurement of the fibre density

Coir fibre is a porous fibre which comprises a high number of lumens in the fibre structure. When the fibres are used in composites, the fibre volume fraction can be calculated by taking into account the whole fibre volume. However, only the solid material of the fibre will carry load during loading of the composite. Consequently, both the density of the whole coir fibre and that of the fibre solid fraction are important for the characterisation of fibre and composite properties. In this experiment, coir fibres were cut to different fibre lengths of 4, 2, 1 and 0.5 mm and also to grinded fibre of approximately 0.05 mm length (considered as solid particles). The samples were weighed to know the mass, and the sample volume was determined using a gas pycnometer (Beckman 930). Accordingly, the density of the samples could be calculated by using the measured mass and volume.

2.4. Single fibre tensile tests

Single technical fibres (which consist of a bundle of structurally bonded elementary fibres) were tested in tension on a mini universal test machine. Because of the small diameter of coir fibres (<0.5 mm), it is practically difficult to measure the fibre strain by using an extensometer, which is usually applicable for tensile testing of larger samples. Therefore, two methods were used to determine the fibre strain in this study.

In the first method, the test was performed on an Instron 5943 integrated with a camera system for optical strain measurement. Speckles were created on the fibre surface so that the camera system could map the fibre strain during tensile loading. It should be noted that the preparation of speckle pattern is very important since the detection and calculation of fibre displacements are based on the speckle pattern. The smaller size and higher density of speckles could provide more effective speckle pattern for the analysis. The recorded strain mapping data were analysed using Limess software and the calculated strains were then linked with the tensile load data to plot the stress–strain curve of the fibres. A 1 kN load cell was used for the test, and the crosshead speed was set at 1 mm/min. It should be noted that the load measurement accuracy of this new Instron machine is quite high (±0.5% of the reading down to 1/500 of the load cell capacity of 1 kN, hence ±10 mN on a total of 2 N) so this provides an accurate measurement even at the low loading forces used. At least 15 fibres were tested in this method.

The second method was based on correction of the fibre slippage and machine compliance. A variety of test span lengths (10, 15, 20, 25, 30 mm) were used for performing the tensile test on a home-made mini tensile machine. For each span length, a minimum of 15 fibres were tested. Based on the obtained data of load and displacement at different span lengths, a theoretical correction (developed by Defoirdt et al., 2010), which is described in the following paragraphs) for the fibre slippage and machine compliance was used to determine the correct strain of the fibre samples. The crosshead speed was set at 1 mm/min and a 200 N load cell was used in this study.

Concerning sample preparation, for both methods, the fibre sample was randomly selected and glued into a paper frame, as shown in Fig. 1. This keeps the fibre as straight as possible and assures a good gripping. Before fixing the fibres in the paper frame, the mass per length was measured for every fibre. The loaded cross-sectional area of the fibre, which was used to convert applied force

Please cite this article in press as: Tran, L.Q.N., et al., Investigation of microstructure and tensile properties of porous natural coir fibre for use in composite materials. Ind. Crops Prod. (2014), http://dx.doi.org/10.1016/j.indcrop.2014.10.064

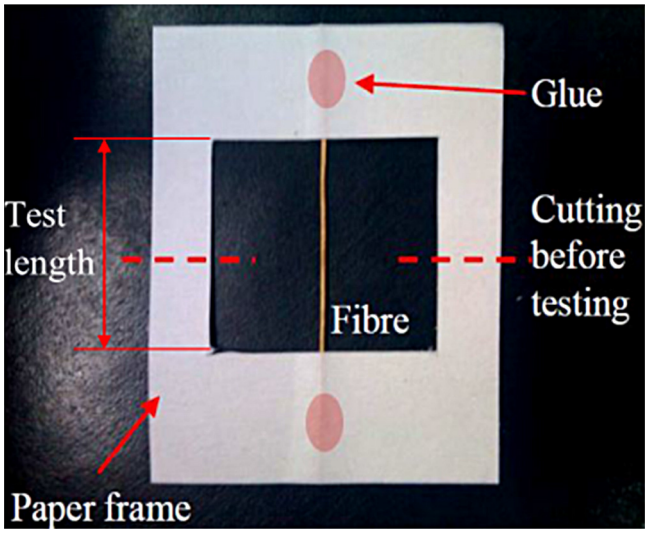

Fig. 1. Paper frame for single fibre tensile test.

to stress, was calculated using the mass, the length and the mean density of the coir fibres. It is important to ermphasize that in this study the density of the solid coir material was used, which means that the equivalent cross-section of the solid material was obtained.

As mentioned, in the second method, the measured displacement will consist of fibre strain, slippage and machine compliance. A correction procedure for slippage and machine compliance developed by Defoirdt et al. (2010) was applied to the correct strain at failure and the *E*-modulus, described as follows:

The strain is expressed in Eq. 2-1:

$$\text{uncorrected strain} = \frac{\Delta l_{\text{total}}}{\text{test length}} = \frac{\Delta l_{\text{fibre}}}{\text{test length}} + \frac{\Delta l_{\text{non-fibre}}}{\text{test length}} \quad (1)$$

where Δl_{total} is the measured displacement of the clamps, Δl_{fibre} is the elongation of the fibre and $\Delta l_{\text{non-fibre}}$ is the displacement caused by slippage and machine compliance.

The key element of this method is that the fibre modulus is determined at infinitely long test length. At infinite fibre length, the displacement that is not caused by the elongation of the fibre can be ignored. The procedure is that the measured (apparent) modulus data from each test are plotted as function of 1/(test length). Then, by (linear) extrapolation to 1/(test length) = 0, the fibre modulus at infinite fibre length can be estimated (E_e).

To correct all the strain values for the effects of slippage and machine compliance, the next step is to estimate a compliance factor α_i for each test; α_i captures the effects of both slippage and machine compliance for each test and is assumed to be a constant for each test.

It can be written for a certain stress σ at the first linear part of the stress–strain curve:

$$\frac{\Delta l_{\text{fibre}}}{\text{test length}} = \frac{\sigma}{E_e} \quad (2)$$

It is assumed that the non-fibre strain is proportional to the load put on the fibre:

$$\frac{\Delta l_{\text{non-fibre}}}{\text{test length}} = \frac{\alpha F}{\text{test length}} \quad (3)$$

where F is the load put on the fibre (which corresponds to the chosen stress σ as mentioned above) and α is the factor that estimates the influence of slippage and the test setup compliance. So, for every tested fibre α_i can be calculated:

$$\alpha_i = \frac{\Delta l_{\text{total},i} - \Delta l_{\text{fibre},i}}{F_i} \quad (4)$$

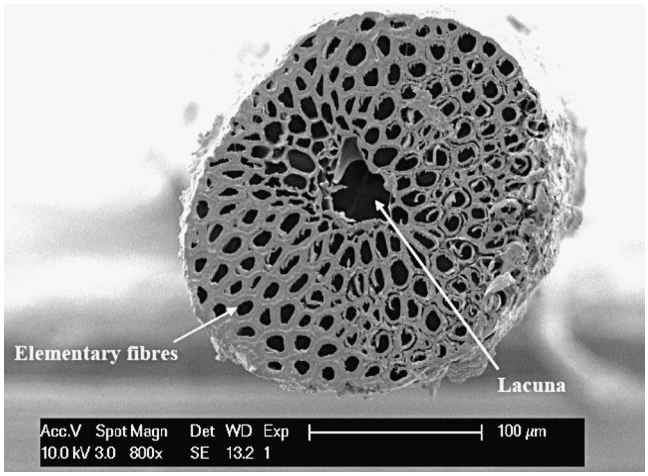

Fig. 2. SEM images of cross-section of a typical coir fibre with presence of lacuna and elementary fibres.

In the ideal case this factor should be the same for all tested fibres and for all measured test lengths. In reality, there is quite some spread. In this work, α value was determined for each test length: all α_i values are plotted versus the test length and by a linear regression, an estimation of the $\alpha_{\text{test length}}$ value for each test length can be determined. With this estimated value for $\alpha_{\text{test length}}$ the corrected strain can be calculated:

$$\text{corrected strain} = \frac{\Delta l_{\text{total},i}}{\text{test length}} - \frac{\alpha_{\text{test length}} F_i}{\text{test length}} \quad (5)$$

With the corrected strain values, the corrected stress–strain curves can be drawn. From these, as a consistency check, it can be verified if the *E*-moduli read from the corrected graphs, correspond to E_e.

3. Results and discussion

3.1. Fibre internal microstructure and porosity

In Fig. 2, a typical cross section of a coir fibre indicates that a technical coir fibre comprises numerous elementary fibres with a lumen inside. The larger hole, which is approximately located in the centre of the technical fibre, is called lacuna.

In the close up images of elementary fibres as seen in Fig. 3a and b, it can be seen that each elementary fibre consists of two cell wall layers which contain bundles of microfibrils, and the middle lamella glues the elementary fibres together. The structure of coir fibres follows the common cell wall structure of wood and plant fibres, but with much larger MFA (Persson, 2000). In the primary wall, the microfibrils seem to be oriented at around 45° to the fibre direction, while the angle is larger (close to 90°) in the secondary wall, as can be observed in Fig. 3b. The secondary wall is somewhat thicker than the primary one. The high angle of the microfibrils in coir fibres is also reported in literature (Martinschitz et al., 2008). Observably, coir fibre is a hollow fibre with quite big lumens and thin walls, and the fibre cross-section is rather circular.

Concerning the porosity of coir fibres, the results from both SEM image analysis and SEM-CT scans are compared. In Fig. 4, a SEM image of the fibre cross section is analysed using the software Leica QWin, and the fibre porous area is detected and calculated. Assuming that the fibre cross section, the lumen and the lacuna are uniform along the fibre, the porosity of the fibre is then calculated based on the ratio of the porous area and the total area of fibre cross section. Using the same principle, the volume fraction of the lacuna in the fibre can also be determined.

Please cite this article in press as: Tran, L.Q.N., et al., Investigation of microstructure and tensile properties of porous natural coir fibre for use in composite materials. Ind. Crops Prod. (2014), http://dx.doi.org/10.1016/j.indcrop.2014.10.064

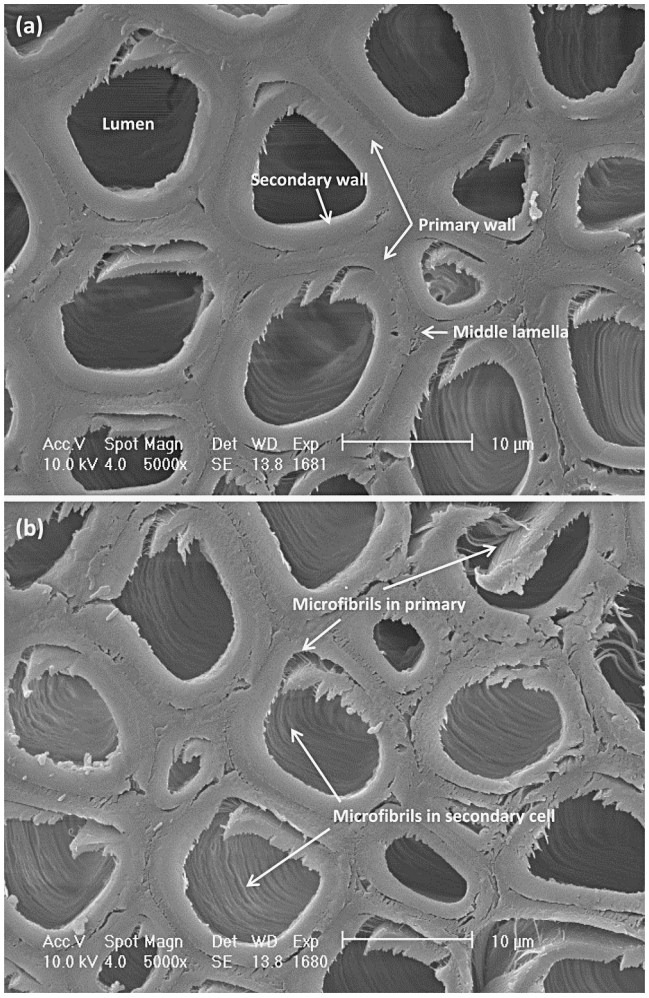

Fig. 3. SEM images of elementary fibres which show (a) different lumen and cell walls and (b) some micro fibrils the primary and secondary cell walls.

The results of all analysed fibres are shown in Table 1. For each fibre, the data are obtained based on the analysis of three different cross sections. To have an idea about the size of the tested fibres, the fibre diameter is approximately determined based on fibre cross sectional area by simply assuming the fibre has a circular cross section. With the SEM method, the results show that the fibre porosity is in the range from 22 to 30%.

Considering the fibre lacuna, its volume fraction in the fibre is around 2–3%. It should be noted that this analysis of fibre porosity has some limitations. In reality, the lumen are not connected between the elementary fibres which are located in the same line along the technical fibre (as seen in Fig. 6). Therefore, the calculation of the volume of lumens based on their cross sectional areas may give some overestimation. On the other hand, the lumen of each elementary fibre is not a cylinder (the cross section of lumen is not uniform, but its cross section is decreasing from the middle to the ends of the elementary fibre). In this case, the volume of lumens can be underestimated when a smaller cross section is analysed. Therefore, the hypothesis has been used that by using 3 random cross-sections, a good approximation of the average lumen size will be obtained (given also the relatively uniform cross-section of the fibres).

In the analysis of the fibre structure using SEM-CT scans, a volumetric data set of scanned fibre samples is reconstructed from scanned images. The structure can be observed by orthogonal virtual slicing through the 3D structure (Fig. 5). It can be seen that the elementary fibres are discontinuous and oriented uni-directionally in the fibre direction. The lumen are also discontinuous and remain inside every individual elementary fibre (Fig. 6). The lacuna is a cylindrical channel in the middle of the technical fibre. With the help of the software SkyScan CTAn, a 3D model of the fibre can be built from the reconstructed data set, and internal structural measurements such as fibre porosity and lacuna volume fraction are carried out. The result of these analyses is also shown in Table 1.

The porosity of the coir fibres (from 10 tested fibres) ranges from 27 to 40%, except the value of fibre number 10, which is approximately 46%. In comparison with the results obtained from the analysis of the SEM images of cross sections, the fibre porosity from this analysis is higher. The method is based on a densitometry principle; the quality of the scanned images depends on the density difference between the fibre solid material and air. Because this difference is not large in case of coir fibre, some errors are included. Besides, coir fibres consist of various thin organic tissues, which may not be detected on the scanned images. Hence, the fibre porosity analysed with this method is likely to be overestimated since the fibre solid material is not fully determined.

In summary, the two discussed methods offer good tools to study the porosity and generally the internal structure of coir fibres. Based on the above discussion, it can be hypothesised that the fibre porosity will be better estimated by image analysis on SEM pictures of fibre cross sections, and hence it will be in the range from 22 to 30%.

Regarding the elementary fibres, using orthogonally sliced SEM-CT images of coir fibre (in longitudinal and transverse direction),

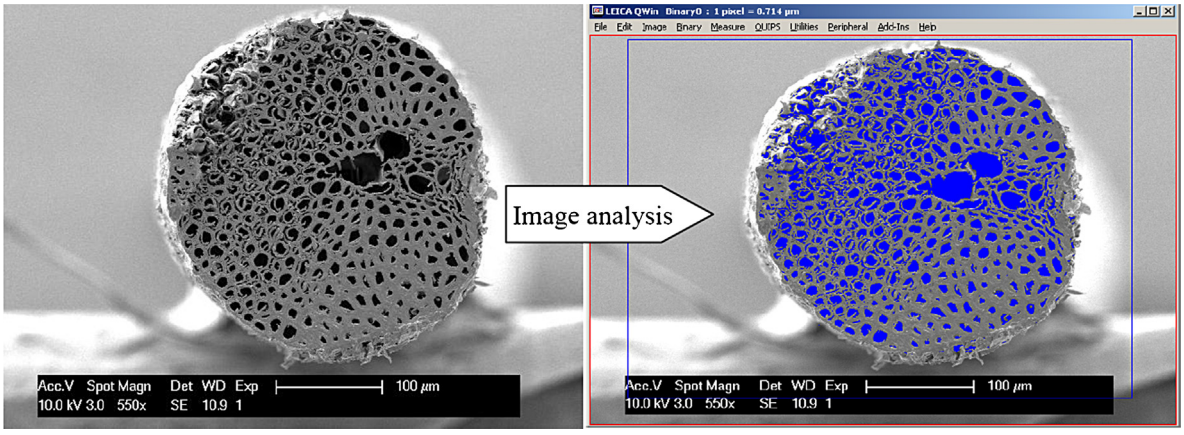

Fig. 4. Image analysis to measure the porous area of the fibre cross-section using the software Leica QWin.

Please cite this article in press as: Tran, L.Q.N., et al., Investigation of microstructure and tensile properties of porous natural coir fibre for use in composite materials. Ind. Crops Prod. (2014), http://dx.doi.org/10.1016/j.indcrop.2014.10.064

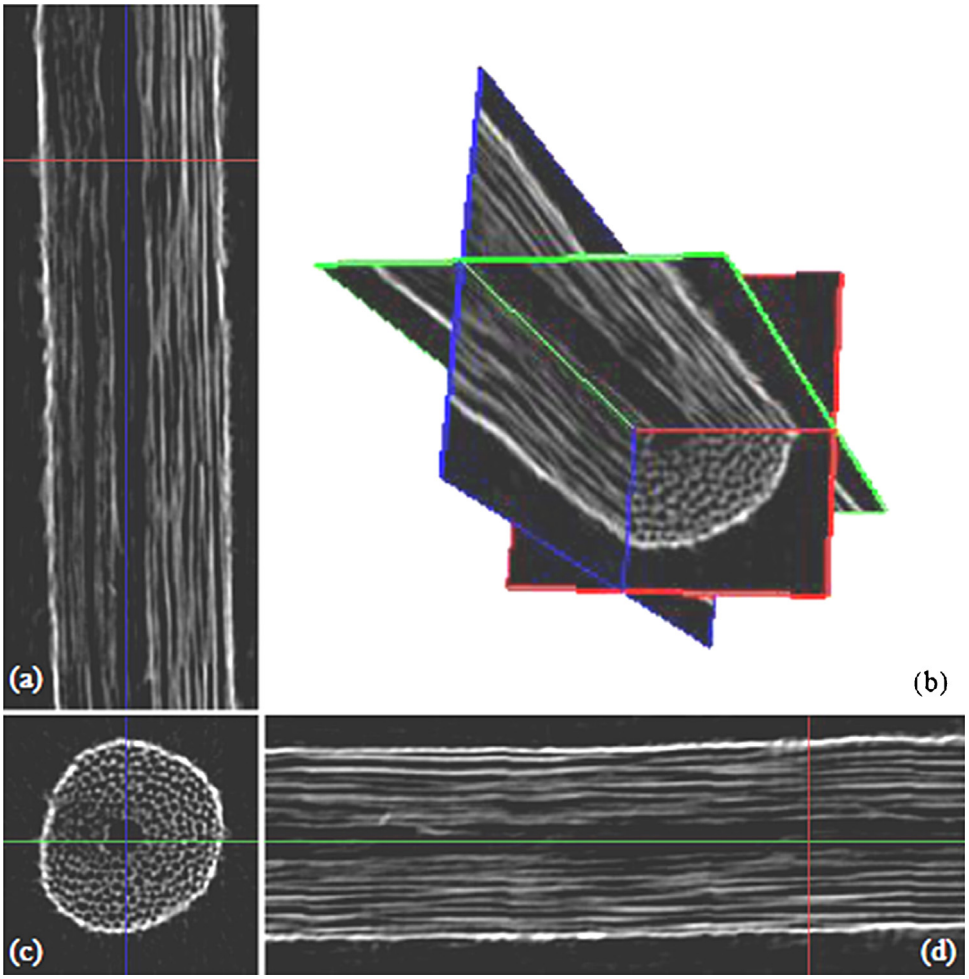

Fig. 5. Three orthogonal virtual slices through a 3D reconstructed internal structure of coir fibre obtained from SEM-CT scanned images, (a) coronal image (b) 3D navigation (c) transaxial image and (d) sagittal image.

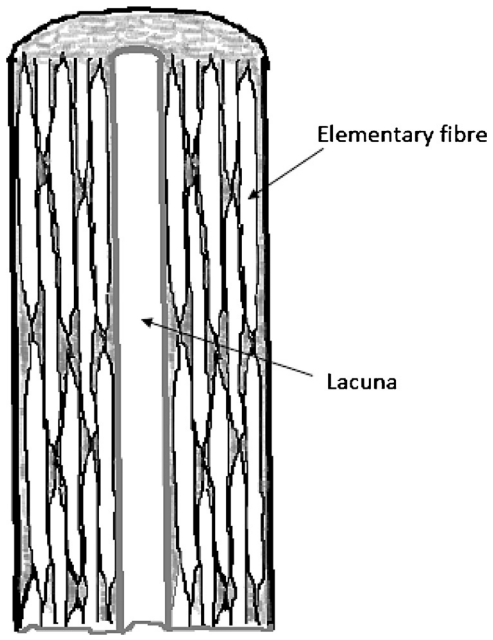

Fig. 6. Schematic presentation of the orthogonal slice of technical coir fibre which shows the organisation of elementary fibres (with lumen) inside the technical fibre.

the length and diameter of elementary fibres can be estimated as shown in Fig. 7. In these images, the vertical section of elementary fibres is seen to have an elliptical shape. Hence, the length of the elementary fibre is approximately equal to the major diameter of this ellipse shape. The diameter of the elementary fibres is determined from the fibre cross section. The results are presented in Table 1.

From the measurement of ten fibres, the length of elementary fibres is in the range of 350–950 μm, which is quite close to the reported values for Philippines' coir, ranging from 700 to 1100 μm (van Dam et al., 2006). The result measured in this study may be underestimated since the analysed vertical sections of elementary fibre may not be from the centre of each fibre. Therefore, it is recommended to rather refer to the higher value in the range as the representative length.

For the average diameter of the elementary fibres, their values range from 6 to 19 μm which depends on their location in the technical fibre. It is observed that the elementary fibres located near the lacuna have a bigger diameter than those close to the edge of the technical fibre. Again here, because the measured values are obtained from a random cross-section, the values are estimations of the average cross-section.

3.2. Density of coir fibres

Fig. 8 presents the density of coir fibre as function of the length of the tested fibre sample, from pycnometer measurements. The

Please cite this article in press as: Tran, L.Q.N., et al., Investigation of microstructure and tensile properties of porous natural coir fibre for use in composite materials. Ind. Crops Prod. (2014), http://dx.doi.org/10.1016/j.indcrop.2014.10.064

Table 1
Porosity of coir fibre determined from SEM image analysis and SEM-CT Scans.

Fibre	Image analysis of fibre cross-section (SEM)					SEM-CT Scan			
	Diameter[a] (μm)	Cross-sectional area (μm²)	Pore area (including lacuna) (μm²)	Lacuna area (μm²)	Total fibre porosity (%)	Lacuna volume fraction (%)	Total fibre porosity (%)	Lacuna volume fraction (%)	Elementary fibre diameter (μm)	Elementary fibre length (μm)
1	282 ± 2.5	62,572 ± 1115	15,229 ± 1130	1745 ± 87	24.3 ± 1.4	2.8 ± 0.2	37.4	2.0	10.2–18.4	428–738
2	301 ± 6.2	71,031 ± 2935	16,356 ± 2786	1374 ± 395	23.1 ± 4.9	1.9 ± 0.5	27.0	3.6	7.9–15.8	364–617
3	219 ± 8.7	37,657 ± 2948	10,990 ± 878	774 ± 120	29.2 ± 1.3	2.1 ± 0.5	32.2	2.6	8.1–14.9	283–568
4	301 ± 13.9	71,008 ± 6477	19,217 ± 4652	2008 ± 976	26.8 ± 4.6	2.8 ± 1.3	37.1	2.5	6.4–15.0	455–960
5	192 ± 11.9	28,895 ± 3581	8233 ± 712	960 ± 43	28.6 ± 2.1	3.4 ± 0.4	32.0	2.4	5.6–15.7	330–763
6	235 ± 6.6	43,234 ± 2437	11,297 ± 440	959 ± 89	26.2 ± 2.4	2.2 ± 0.2	29.6	1.8	6.9–17.8	457–869
7	276 ± 14.2	60,024 ± 6213	18,260 ± 1938	1656 ± 274	30.5 ± 3.0	2.8 ± 0.1	35.2	4.6	6.3–12.9	367–752
8	247 ± 3.2	47,900 ± 1250	14,264 ± 2157	1638 ± 586	29.8 ± 4.2	3.4 ± 1.3	33.4	3.3	8.4–14.9	336–781
9	158 ± 1.0	19,684 ± 254	4142 ± 141	331 ± 111	21.1 ± 1.0	1.7 ± 0.6	39.8	4.0	7.6–18.6	366–551
10	259 ± 10.6	52,881 ± 4298	16,184 ± 1610	1497 ± 721	30.7 ± 3.9	2.9 ± 1.4	46.3	2.1	8.0–19.5	321–668

[a] Fibre diameter is approximately calculated from the area of fibre cross section by assuming it has circular shape.

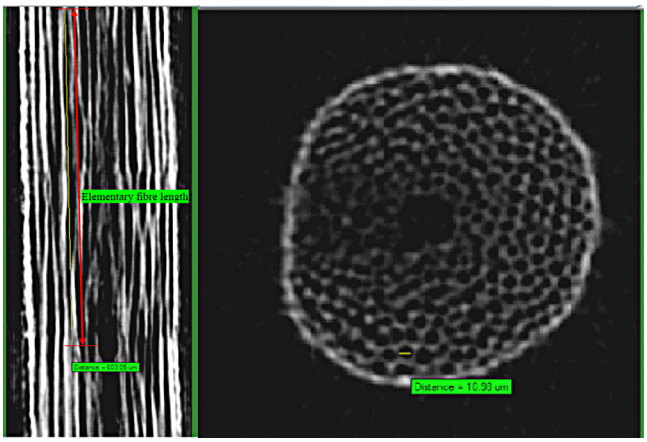

Fig. 7. Measuring the length and diameter of elementary fibres from SEM-CT sliced images. The length of lumens (in black) gives an estimation of elementary fibre length.

results show that the density of solid fibre material measured on grinded powder (estimated length of 0.05 mm) is approximately 1.3 g/cm^3 (in the range of its constituents' density: the cellulose and lignin density are 1.53 g/cm^3 and 1.06–1.33 g/cm^3 respectively). The density decreases to 0.9 g/cm^3 with increasing fibre length, and this value should be considered as the density of structural coir fibre.

The results can be explained considering the internal porous structure of coir fibre. The density of fibre was determined by the ratio of the weight of fibre samples and their volume. At very short length (approximately 0.05 mm), the solid material of coir fibre is characterised. The measured volume is the volume of the fibre solid material. With increasing fibre length, the enclosed porosity (in elementary fibres) of the fibre sample increases. In this case, the measured volume includes the fibre solid volume and the enclosed air volume in elementary fibres. Consequently, the fibre density calculated based on fibre sample volume changes with the change of fibre length. The density will decrease with increasing fibre length because more "closed" porosities will be present in the sample.

Based on this result, the average (lumen) porosity of coir fibres can be derived by the ratio of the fibre air volume and the total fibre volume, which gives about 31%. This result is quite consistent with that obtained from image analysis from SEM images of the cross sections.

3.3. Tensile mechanical properties of coir fibres

As described in Section 2.4, the coir fibres were tested using a tensile machine with an optical strain mapping system. The displacement of the speckles on the fibre surface was captured by the camera, and analysed using the software Vic-2D. Fig. 9a presents

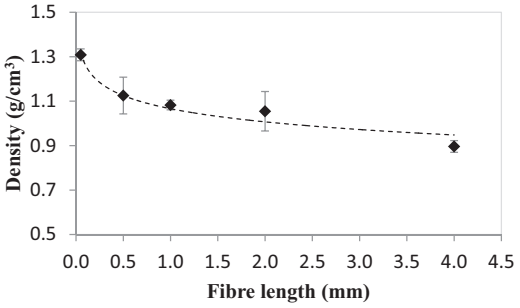

Fig. 8. Density of coir fibre as function of the length of the fibre samples; results from pycnometer measurements.

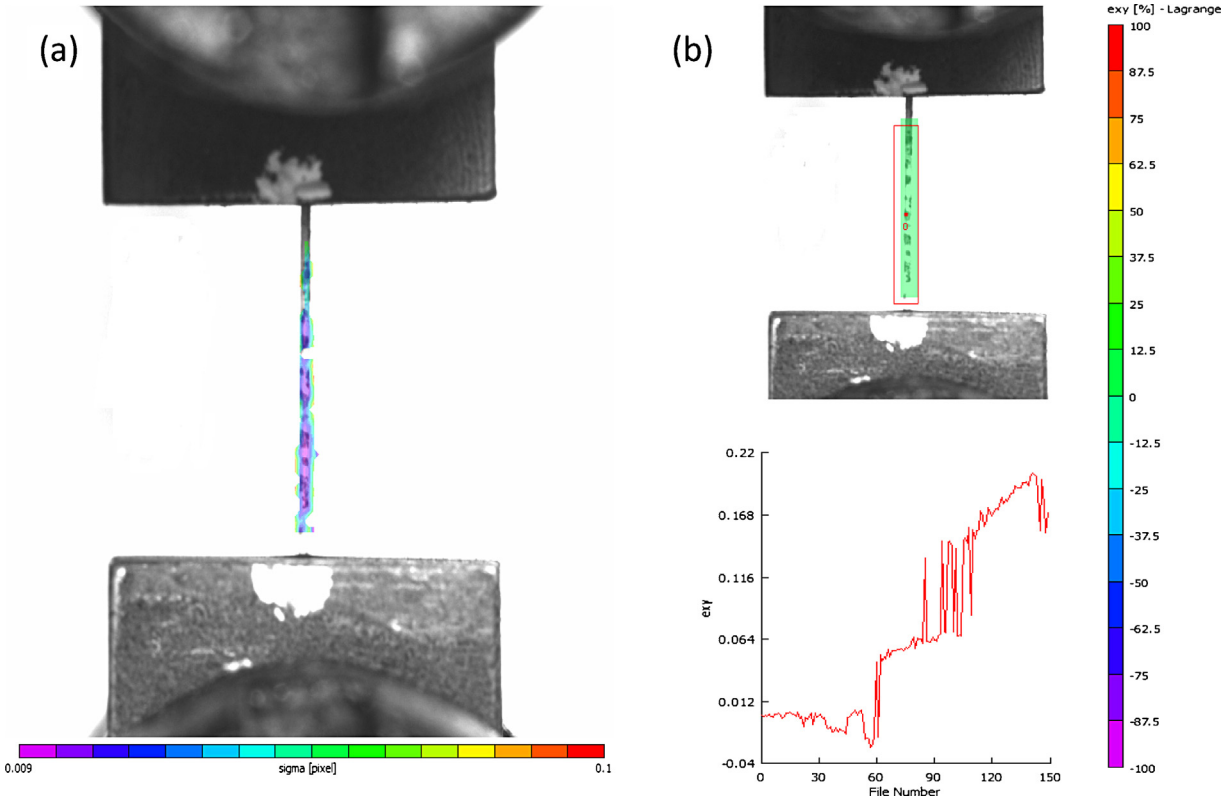

Fig. 9. Optical strain mapping in fibre tensile test (a) image correlation shows fibre displacement mapped by tracking the movement of speckles on the fibre surface and (b) strain distribution of analysed coir fibre and fibre strain calculated by the software Vic-2D.

the image correlation process with tracking the fibre displacement. The strain distribution of the analysed fibre is then defined as shown in Fig. 9b. In order to create a strain distribution map of the fibre, during the deformation of the fibre under tensile loading, a series of images of the fibre surface are captured to evaluate the change of the fibre surface thanks to speckle pattern created on the fibre surface. The differences between speckle patterns can be calculated by correlating all the pixels of the reference image (image taken before loading) and any deformed image.

The strain of each analysed fibre is then linked to the corresponding tensile load recorded by the tensile testing machine to obtain the stress–strain curves (the stress is determined by the ratio of the tensile load and the initial area of fibre solid cross-section which is calculated by using the fibre length and the solid fibre density of 1.3 g/cm^3). The curves show that coir fibre are a linear elastic at low stress, and then shows plastic behaviour until fibre failure at very high strain to failure (Fig. 10).

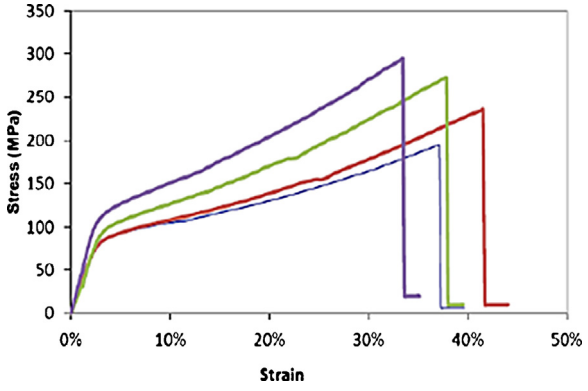

Fig. 10. Typical tensile stress–strain curves of single coir fibres.

The tensile modulus, strength and strain to failure of the coir fibres were calculated and are shown in Table 2. It can be seen that the coir fibres have high strain to failure, but are not so strong and stiff. As known from the analysis of the fibre internal structure, coir fibres have a high MFA, which explains the low stiffness in fibre direction and the high elongation thanks to reorientation of the microfibrils under tensile loading. The properties of the fibres are comparable with previously reported results (Defoirdt et al., 2010; van Dam et al., 2006).

With the procedure using a correction for slippage and machine compliance, by using different test span lengths, the extrapolated *E*-modulus at infinite test length was first obtained by plotting a

Table 2
Tensile *E*-modulus, strength and strain to failure of coir fibre by two different testing methods (optical strain mapping and corrected fibre strain from a range of test lengths); the fibre density used to determine fibre cross-sectional area was1.3 g/cm^3.

A. Optical strain mapping (5 mm test length)	
E-modulus (GPa)	4.6 ± 1.1
Strength (MPa)	234.2 ± 57.4
Strain at failure (%)	18.0–36.7
B. Range of test lengths (10, 15, 20, 25 and 30 mm)	
Extrapolated *E*-modulus (GPa)	4.54
E-modulus from corrected stress–strain curves (GPa)	4.9 ± 0.9
Strength (MPa)	204.6 ± 39.8
Measured strain at failure (smallest test length/longest test length) (%)	44.7 ± 11.4/34.4 ± 4.9
Corrected strain at failure (smallest test length/longest test length) (%)	41.0 ± 10.7/33.5 ± 5.0

Please cite this article in press as: Tran, L.Q.N., et al., Investigation of microstructure and tensile properties of porous natural coir fibre for use in composite materials. Ind. Crops Prod. (2014), http://dx.doi.org/10.1016/j.indcrop.2014.10.064

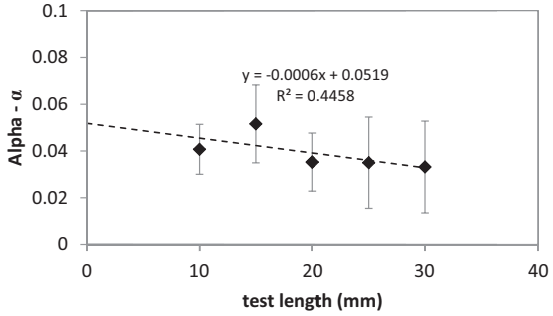

Fig. 11. Alpha values in function of the test length.

trendline of the measured *E*-modulus at different test lengths as shown in Fig. 11a. An extrapolated modulus value of 4.54 GPa was obtained (see also Table 2). Next, the factor α_i was calculated for each tested fibre. Fig. 11 shows average α values for the different test lengths, where the α value depends on the test length. In the study of Defoirdt et al. (2010), it is suggested that α is rather caused by slippage than by test setup compliance. At shorter test lengths, the α values are higher which means the measured extra strain is determined more by slippage in the clamps than by test setup compliance, which should be assumed as constant. Because of the observed variation of the α values, a linear regression line was constructed to obtain the most probable α value for each test length, to correct the fibre strain values.

The corrected strain values were used to construct the corrected stress–strain curves, from which once more *E*-moduli were read. Measured and corrected *E*-moduli are presented in function of the used test lengths in Fig. 12a. The measured modulus is clearly depending on the test length which means that slippage and test setup compliance influence the moduli. After correction, the corrected *E*-moduli are as expected independent on the test length, and the correction is larger at shorter test length. The mean value of the corrected *E*-modulus is around 4.9 GPa which is quite consistent with the value obtained from the optical strain mapping method. The corrected values are a bit higher than the extrapolated modulus of 4.54 GPa, which was the baseline value for the correction procedure. In principle, the corrected values should be exactly the same as the extrapolated value, but the correspondence is believed to be acceptable. The discrepancy can be attributed to the fact that average α values were used in the correction.

In the same manner as the *E*-modulus, the measured strain to failure is dependent on the test length. It can be seen that the corrected strain to failure stays dependent on the test length (Fig. 12b), which is logically linked to the failure probability theory. The longer the fibres, the higher the chance of defects and the earlier they break. The strain to failure at 10 mm test length is approximately 40% which is comparable with the value obtained from the optical strain mapping and literature values at similar test length (Defoirdt et al., 2010; van Dam et al., 2006).

The fibre strength is expected to decrease like the strain to failure when the test length increases following the probability of breakage theory, but it was not observed. The strength seems to stay in a range from 170 to 240 MPa, which is situated in the middle of literature values (Munder and Hempel, 2006; van Dam et al., 2006). Apparently, the defect sensitivity of coir fibres is relatively low. This is logical, as failure is proceeded by massive plastic deformation.

As a conclusion on the test methods, it can be stated that optical strain mapping provides a fast and precise way to determine the fibre elongation during tensile loading, in comparison with the procedure using a correction for slippage and machine compliance, by using different test span lengths. On the other hand, the data at

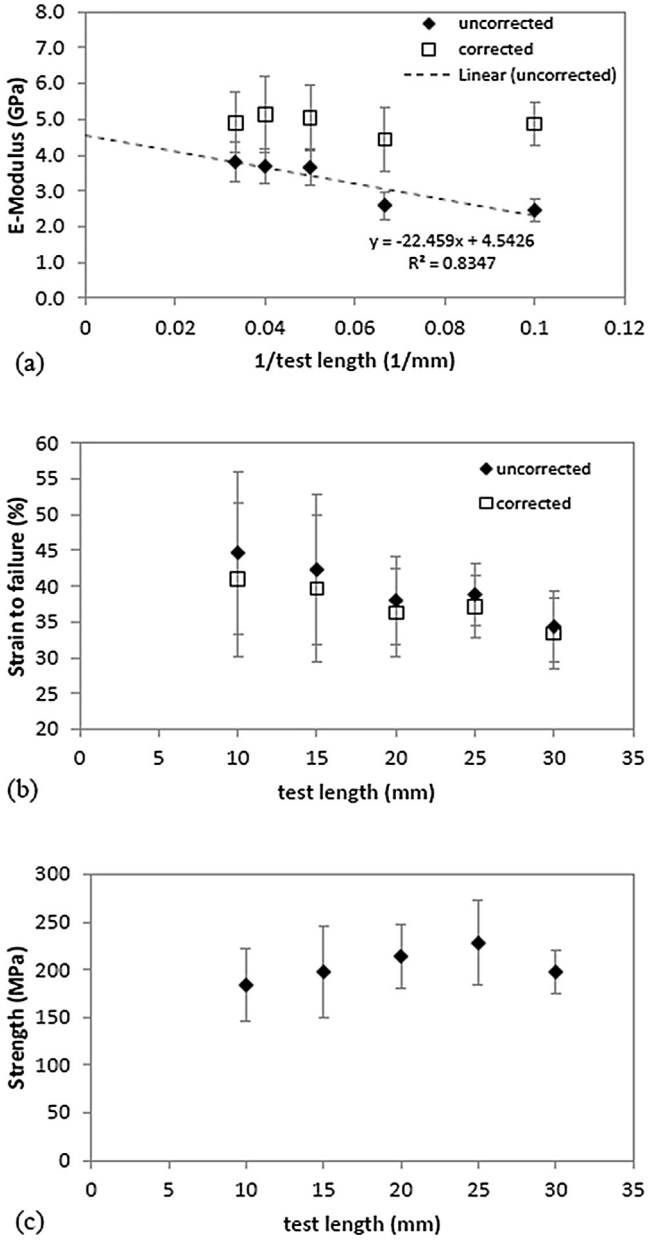

Fig. 12. Tensile properties of coir fibre: (a) uncorrected and corrected *E*-modulus as function of 1/test length, (b) uncorrected and corrected strain and (c) strength as a function of test length.

different test lengths in the latter method give more information about the defect sensitivity of the fibres.

4. Conclusion

The characterisation of the coir fibre cross section using SEM shows that technical coir fibres comprise plenty of elementary fibres (in the range of 200–300 elementary fibres) and a lacuna at the centre. The elementary fibre is built up by two main cell walls which consist of bundles of microfibrils aligned in a high angle to the fibre axis (high microfibril angle). Coir fibre appears to have high porosity at 22–30%.

SEM-CT is a good tool for analysing the internal structure of coir fibre. The fibre porosity and the dimensions of lumen, lacuna and elementary fibres were determined by using 3D information and three orthogonal virtual slices of the scanned fibre. The results confirm that coir fibre has a high porosity.

Please cite this article in press as: Tran, L.Q.N., et al., Investigation of microstructure and tensile properties of porous natural coir fibre for use in composite materials. Ind. Crops Prod. (2014), http://dx.doi.org/10.1016/j.indcrop.2014.10.064

Single fibre tensile testing with optical strain mapping offers a fast (tests are only performed at one test length) and efficient tool to measure tensile properties of coir fibres. The test using different test lengths gives information about the defect sensitivity of the fibres and shows that the defect sensitivity of coir fibres is relatively low. The results of both methods indicate that coir fibres are not very strong and stiff (strength and stiffness are approximately 234 MPa and 4.6 GPa respectively), but have high strain to failure (20–40%), which may increase toughness of composites when they are used as reinforcement for the composites.

By understanding the fibre structure including fibre porosity and fibre mechanical properties, the investigation of coir fibre composite (e.g. fibre volume fraction and mechanical properties of the composite) is more accurate and reliable.

Acknowledgments

The authors wish to thank Gregory Pyka for help in performing SEM-CT scans, and Can Tho University for providing the coir fibres. We also thank KU Leuven and the Belgian Science Policy Department (BelSPO) for supporting our research. Prof. I. Verpoest is holder of the Toray Chair in Composite Materials at KU Leuven.

References

Baley, C., 2002. Analysis of the flax fibres tensile behaviour and analysis of the tensile stiffness increase. Compos. Part A: Appl. Sci. 33, 939–948.
Bledzki, A.K., Gassan, J., 1999. Composites reinforced with cellulose based fibres. Prog. Polym. Sci. 24, 221–274.
Burgert, I., 2006. Exploring the micromechanical design of plant cell walls. Am. J. Bot. 93, 1391–1401.
Chi, Z., Chou, T.-W., Shen, G., 1984. Determination of single fibre strength distribution from fibre bundle testings. J. Mater. Sci. 19, 3319–3324.
Coleman, B., 1958. On the strength of classical fibres and fibre bundles. J. Mech. Phys. Solids 7, 60–70.
Defoirdt, N., Biswas, S., Vriese, L.D., Tran, L.Q.N., Acker, J.V., Ahsan, Q., Gorbatikh, L., Vuure, A.V., Verpoest, I., 2010. Assessment of the tensile properties of coir, bamboo and jute fibre. Compos. Part A: Appl. Sci. 41, 588–595.
Fengel, D., Wegener, G., 1989. Wood: Chemistry, Ultrastructure, Reactions. Walter de Gruyter, Berlin.
Lefeuvre, A.L., Bourmaud, A., Morvan, C., Baley, C., 2014. Elementary flax fibre tensile properties: correlation between stress–strain behaviour and fibre composition. Ind. Crop Prod. 52, 762–769.
Martin, N., Mouret, N., Davies, P., Baley, C., 2013. Influence of the degree of retting of flax fibers on the tensile properties of single fibers and short fiber/polypropylene composites. Ind. Crop Prod. 49, 755–767.
Martinschitz, K.J., Boesecke, P., Garvey, C.J., Gindl, W., Keckes, J., 2008. Changes in microfibril angle in cyclically deformed dry coir fibers studied by in-situ synchrotron X-ray diffraction. J. Mater. Sci. 43, 350–356.
Munder, F., Hempel, H., 2006. Mechanical and thermal properties of bast fibers compared with tropical fibers. Mol. Cryst. Liq. Cryst. 448, 197/[799]-209/[811].
Müssig, J., Stevens, C., 2010. Industrial Applications of Natural Fibres: Structure, Properties and Technical Applications. John Wiley & Sons, United Kingdom.
Navi, P., Rastogi, P.K., Gresse, V., Tolou, A., 1995. Micromechanics of wood subjected to axial tension. Wood Sci. Technol. 29, 411–429.
Osorio, L., Trujillo, E., Van Vuure, A.W., Verpoest, I., 2011. Morphological aspects and mechanical properties of single bamboo fibers and flexural characterization of bamboo/epoxy composites. J. Reinf. Plast. Comp. 30, 396–408.
Page, D.H., El-Hosseiny, F., Winkler, K., 1971. Behaviour of single wood fibres under axial tensile strain. Nature 229, 252–253.
Persson, K., 2000. Micromechanical Modelling of Wood and Fibre Properties. Lund University, Sweden.
Pickering, K., Beckermann, G., Alam, S., Foreman, N., 2007. Optimising industrial hemp fibre for composites. Compos. Part A: Appl. Sci. 38, 461–468.
Silva, G.G., De Souza, D.A., Machado, J.C., Hourston, D.J., 2000. Mechanical and thermal characterization of native Brazilian coir fiber. J. Appl. Polym. Sci. 76, 1197–1206.
Snell, R., Hague, J., Groom, L., 1993. Characterising agrofibers for use in composite materials. In: Proceeding of the 4th International Conference on Woodfiber–Plastic Composites, Madison, WI, pp. 5–11.
Tomczak, F., 2007. Studies on lignocellulosic fibers of Brazil. Part II: Morphology and properties of Brazilian coconut fibers. Compos. Part A: Appl. Sci. 38, 1710.
Trujillo, E., Moesen, M., Osorio, L., Van Vuure, A., Ivens, J., Verpoest, I., 2014. Bamboo fibres for reinforcement in composite materials: strength Weibull analysis. Compos. Part A: Appl. Sci. 61, 115–125.
van Dam, J.E., van den Oever, M.J., Keijsers, E.R., van der Putten, J.C., Anayron, C., Josol, F., Peralta, A., 2006. Process for production of high density/high performance binderless boards from whole coconut husk: Part 2: Coconut husk morphology, composition and properties. Ind. Crop Prod. 24, 96–104.

Please cite this article in press as: Tran, L.Q.N., et al., Investigation of microstructure and tensile properties of porous natural coir fibre for use in composite materials. Ind. Crops Prod. (2014), http://dx.doi.org/10.1016/j.indcrop.2014.10.064